Fu et al. *Zool. Res.* 2024, 45(4): 951−960
https://doi.org/10.24272/j.issn.2095-8137.2024.039

ZR | Zoological Research

Article Open Access

Tumor necrosis factor α deficiency promotes myogenesis and muscle regeneration

Yu Fu[1], Jing-Ru Nie[1], Peng Shang[2], Bo Zhang[1], Da-Wei Yan[3], Xin Hao[1,*], Hao Zhang[1,*]

[1] *State Key Laboratory of Animal Biotech Breeding*, *China Agricultural University*, *Beijing* 100193, *China*
[2] *College of Animal Science*, *Xizang Agricultural and Animal Husbandry University*, *Linzhi*, *Xizang* 860000, *China*
[3] *College of Animal Science and Technology*, *Yunnan Agricultural University*, *Kunming*, *Yunnan* 650201, *China*

ABSTRACT

Tumor necrosis factor α (TNFα) exhibits diverse biological functions; however, its regulatory roles in myogenesis are not fully understood. In the present study, we explored the function of *TNFα* in myoblast proliferation, differentiation, migration, and myotube fusion in primary myoblasts and C2C12 cells. To this end, we constructed *TNFα* muscle-conditional knockout (*TNFα*-CKO) mice and compared them with *flox* mice to assess the effects of *TNFα* knockout on skeletal muscles. Results indicated that *TNFα*-CKO mice displayed phenotypes such as accelerated muscle development, enhanced regenerative capacity, and improved exercise endurance compared to *flox* mice, with no significant differences observed in major visceral organs or skeletal structure. Using label-free proteomic analysis, we found that *TNFα*-CKO altered the distribution of several muscle development-related proteins, such as Hira, Casz1, Casp7, Arhgap10, Gas1, Diaph1, Map3k20, Cfl2, and Igf2, in the nucleus and cytoplasm. Gene set enrichment analysis (GSEA) further revealed that *TNFα* deficiency resulted in positive enrichment in oxidative phosphorylation and MyoD targets and negative enrichment in JAK-STAT signaling. These findings suggest that *TNFα*-CKO positively regulates muscle growth and development, possibly via these newly identified targets and pathways.

Keywords: TNFα; Muscle-conditional knockout; Myogenesis; Regeneration; Muscle development

INTRODUCTION

Tumor necrosis factor α (TNFα) is a cytokine that exists in secreted, membrane-bound, or intracellular soluble forms, exhibiting biological activities across various cell types (Horiuchi et al., 2010; Kriegler et al., 1988). By binding to receptors on the cell membrane, it activates different cascading signaling pathways to regulate processes such as cell growth, differentiation, apoptosis, and inflammatory responses (Jang et al., 2021). Skeletal muscle formation primarily depends on complex processes such as myoblast proliferation, migration, differentiation, cytoskeletal rearrangement, and myotube fusion, which are regulated by multiple genes. Although *TNFα* has been extensively studied in the context of immunology, recent studies have also highlighted its significant roles in skeletal muscle development, including myogenesis, muscle repair, muscle disease, and muscle atrophy (Di Credico et al., 2023; Fang et al., 2021; Li et al., 2020; Shirakawa et al., 2021).

As an endogenous muscle factor, *TNFα* is expressed in cultured myoblasts and strongly activated in injured muscle tissue (Collins & Grounds, 2001; Li & Schwartz, 2001). However, its role in myoblast proliferation and muscle regeneration remains controversial. Overexpression of *TNFα* can substantially reduce the number of $Pax7^+$ cells (Li et al., 2020). Conversely, the exogenous addition of *TNFα* protein can stimulate myoblast proliferation and satellite cell activation (Alvarez et al., 2020; Li, 2003; Shirakawa et al., 2021). Muscle regeneration is impaired in both *TNFα* knock-in mice (Li et al., 2020) and *TNFα* receptor double-knockout mice ($p55^{-/-}p75^{-/-}$) following cardiotoxin (CTX)-induced muscle injury (Chen et al., 2005). Furthermore, *TNFα* consistently inhibits the accumulation of muscle-specific proteins in differentiated C2C12 cells. Notably, it promotes MyoD degradation through the ubiquitin-proteasome pathway, reducing the half-life and abundance of the MyoD protein (Langen et al., 2004). *TNFα* also suppresses myotube formation (Meyer et al., 2015). Interestingly, low concentrations of exogenous TNFα protein can promote myogenesis, while high concentrations induce the opposite effect (Chen et al., 2007). Additionally, triptolide can prevent lipopolysaccharide-induced skeletal muscle atrophy by gradually reducing *TNFα* levels (Fang et al., 2021).

Received: 06 February 2024; Accepted: 07 April 2024; Online: 08 April 2024

Foundation items: This work was supported by the Xizang Major Science and Technology Project (XZ202101ZD0005N), Yunnan Major Science and Technology Project (202302AE090015), National Key R&D Program of China (2023ZD04044-04), and National Natural Science Foundation of China (32060736)

*Corresponding authors, E-mail: haoxin0331@163.com; hzhang@cau.edu.cn

However, the physiological role of *TNFα* in skeletal muscle development and associated molecular mechanisms remain unclear.

Regarding immunity, there is a well-established consensus on the role of the TNFα signaling pathway. The binding of TNFα to its receptor ultimately leads to NF-κB-dependent cellular responses, cell apoptosis, or necrosis (Hsu et al., 1995; Li & Schwartz, 2001; Pasparakis & Vandenabeele, 2015; Varfolomeev & Vucic, 2018). TNFα also activates three groups of MAP kinases, including extracellular signal-regulated, p38 MAP, and c-Jun NH2-terminal kinases (Sabio & Davis, 2014). However, these known signaling pathways do not fully explain the mechanisms by which TNFα regulates muscle development. Therefore, it is plausible that additional, muscle-specific regulatory pathways remain undiscovered and warrant further research.

In the current study, we explored the role of *TNFα* and its associated mechanisms in muscle development. We systematically examined the effects of *TNFα* on myoblast proliferation, migration, differentiation, and myotube fusion. We successfully established *TNFα* muscle-conditional knockout (*TNFα*-CKO) mice *in vivo* and evaluated their skeletal muscle development, muscle regenerative capacity following CTX-induced damage, and exercise endurance. Mechanistically, we identified potential new targets and pathways influenced by *TNFα*. Our results provide a theoretical foundation for further studies on the regulation of muscle development by *TNFα* and propose a novel strategy for myopathy treatment.

MATERIALS AND METHODS

C2C12 cell culture and RNA interference

The C2C12 myoblast cell line (Type Culture Collection of the Chinese Academy of Sciences, China) was cultured in Dulbecco's modified Eagle medium (DMEM, Gibco, USA) with 10% fetal bovine serum (FBS, Gibco, USA) and 1% penicillin/streptomycin (Gibco, USA). To induce differentiation, the cells were incubated in DMEM supplemented with 2% horse serum (Gibco, USA) and 1% penicillin/streptomycin. To interfere with *TNFα* expression, we designed small interfering RNAs (siRNAs) based on the *TNFα* gene sequence and selected the top candidates with the highest scores (siRNA-403, siRNA-509, siRNA-631) from the design website. The number assigned to each siRNA corresponds to its position relative to the start site of *TNFα*. The *TNFα* siRNA sequences were: siRNA-403, sense: CUCAGAUCAUCUUCUCAAATT, antisense: UUUGAGAAGAUGAUCUGAGTT; siRNA-506, sense: CCAACGGCAUGGAUCUCAATT, antisense: UUGAGA UCCAUGCCGUUGGTT; and siRNA-631, sense: AGCCG AUUUGCUAUCUCAUTT, antisense: AUGAGAUAGCAAAU CGGCUTT. Cell transfection was performed using Lipofectamine 2000 in accordance with the manufacturer's instructions (Invitrogen, USA).

Animals

The *floxed-TNFα* mouse line (C57BL/6N background) was established by Cyagen Biosciences (China) by inserting LoxP site flanking exons 1 and 4 of the *TNFα* gene. The *TNFα*-CKO were generated by crossing $TNF\alpha^{flox/flox}$ and *Myf5-Cre* mice obtained from Jackson Laboratory (USA). The mouse genotype was determined via polymerase chain reaction (PCR) using tail DNA with the following primers: *Cre*-F: 5′-AACCAGAGACTCCCCAAGGT-3′, *Cre*-R: 5′-ACGAAGTTATT AGGTCCCTCGAC-3′, *Cre*-WR: 5′-CGGCTCTTAAAGCAAT GGTC-3′, F2: 5′-GAGACCTAAGCTCTATCCCTGCTC-3′, R2: 5′-TCACATTTTCAGCCCTGTGTCTTT-3′). Cre^{-} mice had an amplicon of 240 bp, while Cre^{+} mice possessed an amplicon of 120 bp. Furthermore, $flox^{+/+}$ mice showed a single band at 205 bp, while $flox^{-/-}$ mice showed a single band at 138 bp. Consequently, $flox^{+/+}Cre^{-}$ mice served as control $TNF\alpha^{flox/flox}$ mice, while $floxflox^{+/+}Cre^{+}$ represented *TNFα*-CKO mice. For muscle regeneration assays, 50 μL of CTX (20 μmol/L, Sigma-Aldrich, USA) was injected into the tibialis anterior (TA) muscles of 2-month-old mice. All animal procedures were performed in accordance with the guidelines for good laboratory practice. The animals were provided with sufficient water, standard chow diet, and appropriate feeding conditions. Furthermore, the animal care and experimental procedures were conducted based on the National Research Council Guide for the Care and Use of Laboratory Animals and were approved by the Institutional Animal Care and Use Committee at China Agricultural University, Beijing, China (approval number: AW80203202-1-1).

Primary myoblast purification and culture

Mouse primary myoblasts were isolated from 6-week-old C57BL/6N mice. Briefly, mouse muscles were minced and digested in 0.2% type II collagenase (Sigma-Aldrich, USA) and 2.5 U/mL dispase (Roche Applied Science, USA) for 1 h. After digestion, the cells were filtered and centrifuged at 1500 ×*g* for 5 min at room temperature, then cultured in growth medium (F10 supplemented with 20% FBS, 1% penicillin-streptomycin, 5 ng/mL basic fibroblast growth factor, and 1% chicken embryo extract) on collagen-coated cell culture plates at 37℃ and 5% CO_2.

EdU and CCK8 assays

5-Ethynyl-2-deoxyuridine (EdU) and Cell Counting Kit-8 (CCK8) assays were conducted in accordance with the instructions provided with the EdU (Ribobio, China) and CCK8 (Solarbio, China) assay kits, respectively. In the EdU assay, cells transfected for 24 h were incubated with 50 μmol/L EdU for 2 h, then fixed with 4% paraformaldehyde (PFA), permeabilized with 0.5% Triton X-100, and incubated with Apollo reaction buffer. EdU-labeled cells and 4',6-diamidino-2-phenylindole (DAPI)-stained (Solarbio) nuclei were photographed under a microscope (ZEISS, Germany). For the CCK8 assay, transfected cells were incubated with 100 μL of 10% CCK8 solution at 37℃ for 1 h. Absorbance was measured at 450 nm using a multimode reader (Biotek, USA).

Cell wounding and Transwell migration

For wounding, the cells (24–48 h after transfection) were scratched with a pipette tip of the same width. Floating cells were washed with phosphate-buffered saline (PBS) and the medium was then replaced with DMEM plus 2% FBS. At 24 h post-wounding, cell migration distance was recorded. For the Transwell assay, equal amounts of cells were cultured in the lower and upper Transwell chambers for 12 h, with crystal violet then used to stain the migrated cells induced by the serum gradient.

Immunofluorescence (IF)

Myoblasts or muscle tissues were fixed in 4% PFA for 20 min and permeabilized for 15 min in 0.3% Triton X-100 with PBS. The samples were then blocked in blocking buffer (Beyotime, China) for 2 h at room temperature and incubated overnight at 4℃ with the following primary antibodies: MyHC (M4276,

1:200; Sigma-Aldrich, USA), eMyHC (F1.652, 1:50; Developmental Studies Hybridoma Bank, USA), and laminin (L9393, 1:1 000; Sigma-Aldrich, USA). After incubation, the samples were washed with PBS and incubated with fluorescently labeled secondary antibodies (SA00013-2 and SA00013-3, 1:400; Proteintech, USA) for 1 h at room temperature in darkness. The samples were then washed with PBS and the cell nuclei were labeled using DAPI for 5 min. Finally, immunofluorescence images were visualized using a fluorescence microscope (Model Q500MC; Leica Image Analysis System, Germany).

Magnetic resonance imaging (MRI)

MRI was performed under anesthesia using 2% isoflurane on an MRI system equipped with a 7 T/16-cm wide-bore instrument. Thus, 20 contiguous coronal slices (thickness=1 mm), covering the region from the knee to the ankle, were acquired. The scan parameters were: echo time (TE)=7.8 ms, repetition time (TR)=500 ms, field of view=100 mm×60 mm, matrix size=256×256, and acquisition time=20 min. The images were analyzed using VNMRJ v.4.0 (Varian Associates, USA).

Hematoxylin-eosin staining (H&E)

After fixation in 4% PFA, tissues were processed for routine paraffin histology and stained with H&E. The sections were then examined under an inverted microscope.

Swimming exhaustion test

Several large beakers were filled with water and maintained at a constant temperature of 28℃. The mice were fasted overnight (15 h), and a piece of metal (7% of body weight) was attached to their tails to ensure that they would sink without swimming. The duration each mouse swam until exhaustion was recorded.

qPCR analysis

Total RNA was isolated from myoblasts and muscle tissues using a TRNzol Universal Reagent (Tiangen, China). Subsequently, 2 μg of total RNA was reverse transcribed into cDNA using a FastKing gDNA Dispelling RT SuperMix Kit (Tiangen, China) according to the manufacturer's instructions. qPCR was then performed using the Universal SYBR Green Fast qPCR Mix system (ABclonal, China). The primer sequences used are shown in Supplementary Table S1.

Western blot analysis

The C2C12 cells and primary myoblasts were lysed in RIPA buffer (Beyotime, China) or a nuclear/cytoplasmic protein extraction kit (Beyotime, China). Proteins were then resolved using sodium dodecyl-sulfate polyacrylamide gel electrophoresis (SDS-PAGE) and transferred to polyvinylidene fluoride (PVDF) membranes. The membranes were then blocked in QuickBlock buffer (Beyotime, China) for 30 min at room temperature and incubated overnight at 4℃ with primary antibodies, including: mouse anti-MyoG (ab1835, 1:500; Abcam, USA), mouse anti-MyHC (M4276, 1:1 000; Sigma-Aldrich, USA), rabbit anti-TNFα (A11534, 1:1 000; ABclonal, China), mouse anti-Casz1 (sc-398303, 1:1 000; Santa Cruz Biotechnology, USA), rabbit anti-Hira (A12527, 1:1 000; ABclonal, China), rabbit anti-Diaph1 (A11596, 1:1 000; ABclonal, China), rabbit anti-Tnnt1 (A10354, 1:1 000; ABclonal, China), rabbit anti-Fgf21 (A3908, 1:2 000; ABclonal, China), rabbit anti-Map3k20 (A14513, 1:1 000; ABclonal), rabbit anti-Cfl2 (A8009, 1:2 000; ABclonal, China), rabbit anti-Histone H3 (A2348, 1:5 000; ABclonal, China), rabbit anti-GAPDH (2118s, 1:5 000; Cell Signaling Technology, USA), and rabbit anti-β-Tubulin (ab6046, 1:5 000; Abcam, USA). Incubation with the secondary antibodies was performed for 1 h at room temperature.

Proteomic analysis

Flox and *TNFα*-CKO primary myoblasts were induced to differentiate for 2 d. Thereafter, nuclear and cytoplasmic proteins were extracted using nuclear/cytoplasmic protein extraction kits (Beyotime, China). Briefly, the samples were sonicated three times with 1% protease inhibitor cocktail on ice using a high intensity ultrasonic processor (Scientz, China). The supernatant was then obtained via centrifugation at 12 000 ×*g* and 4℃ for 10 min. Protein concentration was measured using a BCA kit (Beyotime, China).

The protein samples were added to four volumes of pre-cooled acetone and precipitated at −20℃ for 2 h. Thereafter, they were re-dissolved in 200 mmol/L triethylammonium bicarbonate and ultrasonically dispersed. Trypsin was added at a 1:50 trypsin-to-protein mass ratio for the first digestion overnight. The samples were then reduced with 5 mmol/L dithiothreitol for 30 min at 56℃ and alkylated with 11 mmol/L iodoacetamide for 15 min at room temperature in the dark.

To dissolve and separate the tryptic peptides, an EASY-nLC 1200 UPLC system (Thermo Fisher Scientific, USA) was used at a constant flow rate of 500 nL/min. The separated peptides were then analyzed using an Orbitrap Exploris 480 mass spectrometer (Thermo Fisher Scientific, USA) with a nano-electrospray ion source. The resulting tandem mass spectrometry (MS/MS) data were processed using the Proteome Discoverer search engine (v.2.4.1.15, Thermo Fisher Scientific, USA). The MS/MS data were searched against the Mus_musculus_10090_SP_20230103.fasta database (17 132 entries) concatenated with the reverse decoy database. Trypsin (Full) was specified as the cleavage enzyme, allowing up to two missed cleavages. The false discovery rates (FDRs) for proteins, peptides, and peptide-spectrum match were adjusted to < 1%. The minimum peptide length was set to 6. Label-free measurements were performed using the PTM Bio System (PTM-Biolabs, China). Data were obtained via ProteomeXchange with the identifier PXD046525.

Gene lists were analyzed using GSEA v.4.3.2 from the Broad Institute (Subramanian et al., 2005). The submitted gene list was normalized by applying the $-\log_{10}$ transformation to the count values, assigned as positive or negative based on the direction of the fold change. All other GSEA parameters were set to default. The annotated HALLMARK, DELASERNA, and KEGG gene sets obtained from the DAVID and MSigDB databases were used as enrichment inputs.

Statistical analysis

All data were analyzed using SPSS v.22.0 (IBM, USA) and presented as mean±standard deviation (SD). *P*-values were calculated by performing a two-tailed Student's *t*-test, and statistical significance was indicated as follows: *: $P<0.05$, **: $P<0.01$, and ***: $P<0.001$.

RESULTS

***TNFα* knockdown promoted cell proliferation, migration, differentiation, and myotube fusion in C2C12 cells**

Skeletal muscle formation primarily relies on processes such as myoblast proliferation, migration, differentiation, and

myotube fusion. We successfully reduced *TNFα* expression in C2C12 cells using RNA interference fragments, with siRNA-631 showing the highest interference efficiency (Figure 1A). Regarding proliferation, the CCK8 assay showed higher absorbance for the siRNA-*TNFα* (si-*TNFα*) transfection group than for the siRNA negative control group (si-NC) (Figure 1B). *TNFα* knockdown also significantly increased the number of EdU$^+$ cells (Figure 1C) and up-regulated the expression of proliferation marker genes, *Ki67*, *Cyclin B*, and *CDK4* (Figure 1D). Cell wounding (Figure 1E) and Transwell (Figure 1F) assays demonstrated that *TNFα* knockdown enhanced myoblast migration and promoted C2C12 cell differentiation into more numerous, longer, and thicker myotubes (Figure 1G), with most myotubes exhibiting multi-nucleation (as indicated by white arrows in Figure 1H). *TNFα* knockdown also significantly up-regulated the expression of myogenic marker genes, *MyoG* and *MyoD* (Figure 1I), as well as fusion marker genes, *β-1 integrin* and *Myomaker* (Figure 1J). Muscle hypertrophy and degradation are crucial processes in muscle development (Bodine et al., 2001). Here, the qPCR results showed that *TNFα* knockdown significantly promoted the expression of muscle hypertrophy genes (*Fst* and *Nog*), while inhibiting the expression of *myostatin* and muscle degradation marker genes (*Atrogin1*, *Bmp4*, and *Foxo3*) (Figure 1K). Overall, *TNFα* knockdown promoted myoblast proliferation, migration, differentiation, and fusion in C2C12 cells, implying that *TNFα* plays a significant regulatory role in the growth and development of skeletal muscles.

TNFα-CKO accelerated mouse muscle development, improved exercise endurance, and enhanced muscle regenerative capacity

To investigate the role of *TNFα* in muscle development, we generated conditional knockout mice by selectively deleting *TNFα* in skeletal muscles using *Myf5-Cre/TNFα* and *flox/flox* alleles. The *TNFα*-CKO mice exhibited normal birth and survival, with no apparent abnormalities in appearance (Figure 2A). The male *TNFα*-CKO mice demonstrated significantly higher body weights (Figure 2B) and body lengths (Figure 2C) than the *flox* control mice, while the female *TNFα*-CKO and *flox* mice showed no significant differences in body length (Supplementary Figure S1A). Additionally, the *TNFα*-CKO mice developed more robust forelimbs and hindlimbs (Figure 2D). MRI analysis revealed an increase in hindlimb muscles and subcutaneous fat content in *TNFα*-CKO mice, with no significant changes in skeletal volume between the two groups (Figure 2E). Furthermore, the muscle weights of quadriceps (Quad), tibialis anterior (TA), extensor digitorum longus (EDL), gastrocnemius (GAS), soleus (SOL), trapezius (Trap), and triceps were higher in 2-month-old *TNFα*-CKO

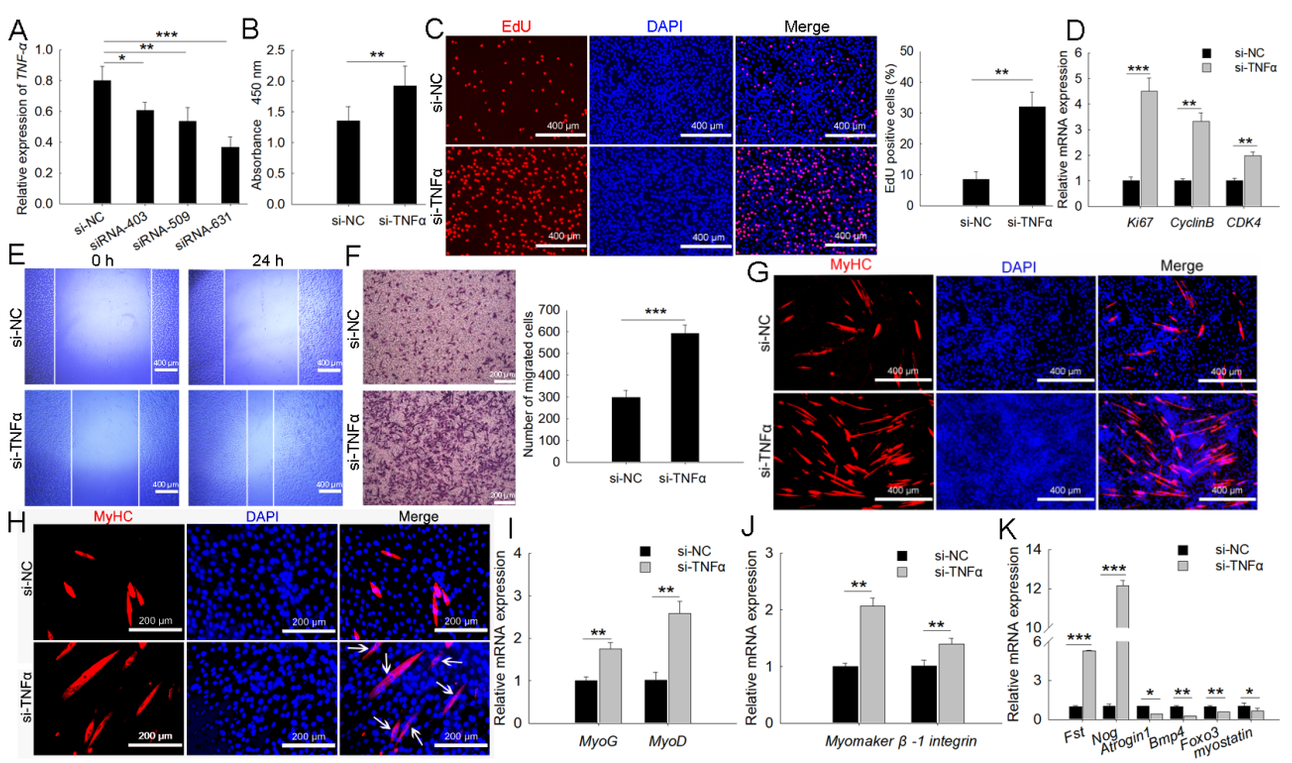

Figure 1 Promotion of myoblast proliferation, migration, differentiation, and myotube fusion in C2C12 cells through *TNFα* knockdown

A: Detection of interference efficiency for different siRNA-*TNFα* fragments. Cells were transfected for 24 h, then collected for qPCR. B: CCK8 assay of si-NC and si-*TNFα* C2C12 cells. C: Representative photographs of EdU-stained si-NC and si-*TNFα* cells. EdU$^+$ staining (red) of S-phase cells and DAPI staining (blue) of cell nuclei are shown (Scale bar: 400 μm), and proliferative cells were quantified as a ratio of EdU$^+$/DAPI$^+$. D: Analysis of expression levels of proliferation marker genes. C2C12 cells were transfected with si-NC and si-*TNFα* for 24 h, then collected for qPCR. E, F: Cell wounding (E) and Transwell (F) analysis of migration ability of myoblasts. Migrated cells were stained purple with crystal violet and counted. G: Immunofluorescence staining for MyHC (red) in si-NC and si-*TNFα* C2C12 cells after culturing for 4 d in differentiation medium (Scale bar: 400 μm). H: Myoblast fusion analysis via immunofluorescence staining for MyHC. White arrows represent multinucleated myotubes (Scale bar: 200 μm). I–K: Analysis of expression levels of myogenic differentiation (I), fusion (J), hypertrophy, and degradation marker genes and *myostatin* (K) in si-NC and si-*TNFα* C2C12 cells using qPCR. Transfected cells were cultured in differentiation medium for 4 d. Data are presented as mean±standard deviation (SD); n=3. *: P<0.05; **: P<0.01; ***: P<0.001 (Student's t-test).

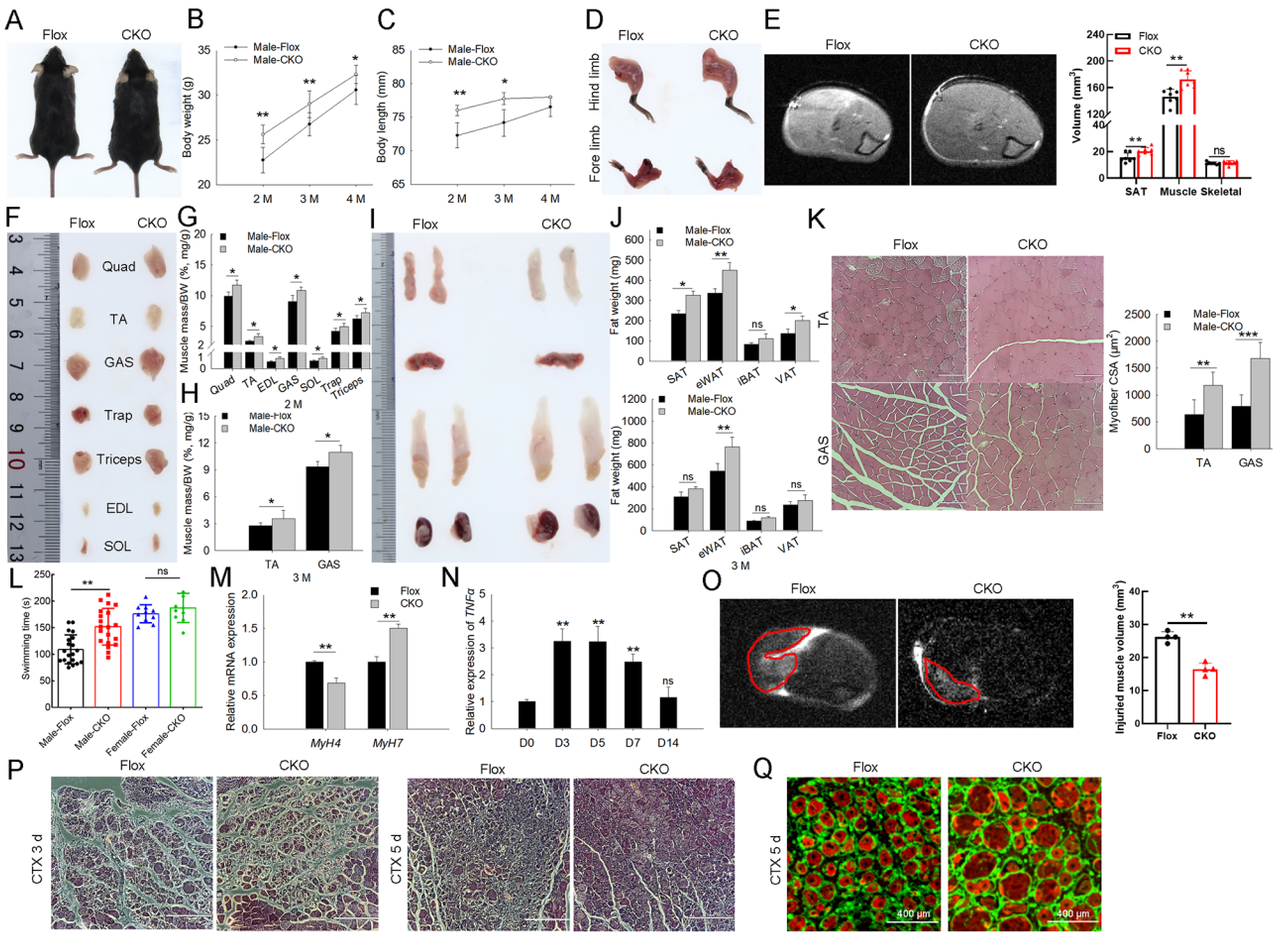

Figure 2 Improved development speed, exercise endurance, and regeneration ability of *TNFα*-CKO mouse muscles

A: Gross body morphology of *TNFα*-CKO and *flox* mice. B, C: Body weight (B) and length (C) of *TNFα*-CKO and *flox* male mice at 2, 3, and 4 months (n≥50). D: Representative photographs of forelimbs and hindlimbs of *TNFα*-CKO and *flox* mice. E: Magnetic resonance imaging (MRI) of hindlimbs, subcutaneous fat (SAT), muscle, and bone volume. F–H: Representative photographs (F) and weight analysis (G and H) of skeletal muscles of *TNFα*-CKO and flox mice. BW, body weight. I, J: Representative photographs (I) and weight analysis (J) of adipose tissue in *TNFα*-CKO and *flox* mice. K: H&E staining of TA and GAS muscles in *TNFα*-CKO and *flox* mice (Scale bar=100 μm). CSA, cross-sectional area. L: Swimming exhaustion time assay for *TNFα*-CKO and *flox* mice (n≥10). M: Analysis of expression level of *Myh4* in EDL and *Myh7* in SOL using qPCR. Mice were sacrificed immediately after swimming exhaustion tests to collect SOL samples. N: Analysis of expression level of *TNFα* after CTX-induced injury at d 0, 3, 5, 7, and 14. O: MRI results and damage volume data 5 d after CTX-induced injury. Area circled by red line indicates damaged muscle tissue (n=6). P: H&E staining of GAS 3 and 5 d after CTX-induced injury (Scale bar=210 μm). Q: Immunofluorescence staining for MyoG (red) and laminin (green) in GAS 5 d after CTX-induced injury (Scale bar=400 μm). Data are presented as mean±SD (n=6). *: P<0.05; **: P<0.01; ***: P<0.001; ns: Not significant (Student's t-test).

male mice than in 2-month-old male *flox* mice (Figure 2F and 2G). Examination of TA and GAS weights in 3-month-old mice showed similar results to those obtained at 2 months (Figure 2H). Muscle weight analyses for female and male *TNFα*-CKO mice were similar (Supplementary Figure S1B). Subcutaneous fat (SAT), epididymal white adipose tissue (eWAT), and perirenal white adipose tissue (pWAT) weights were also significantly increased in 2- and 3-month-old *TNFα*-CKO mice, while differences in interscapular brown adipose tissue (iBAT) weight were not significant (Figure 2I, J). The change in fat tissue weight in female *TNFα*-CKO mice was similar to that in male mice at 3 months, although this was not the case for male and female mice at 2 months (Supplementary Figure S1C). Heart, liver, spleen, lung, and kidney weights revealed that *TNFα*-CKO did not affect the development of major visceral organs in either male or female mice (Supplementary Figure S1D, E). Thus, *TNFα*-CKO accelerated skeletal muscle development and adipose tissue formation, which may be responsible for the changes in mouse body weight observed in this study.

The H&E staining results revealed larger GAS and TA muscle fiber cross-sectional areas in *TNFα*-CKO mice (Figure 2K), consistent with the greater muscle weight observed. A well-developed skeletal muscle system is often associated with endurance. As expected, swimming exhaustion tests showed significantly improved endurance for male *TNFα*-CKO mice. Interestingly, however, no significant differences in endurance were observed between female *TNFα*-CKO and *flox* mice (Figure 2L). *TNFα*-CKO also significantly down-regulated the expression of the fast-twitch muscle fiber marker *Myh4* and up-regulated the expression of the slow-twitch muscle fiber marker *Myh7* (Figure 2M). These findings suggest that *TNFα*-CKO accelerates the development of mouse skeletal muscles and enhances endurance.

Muscle regenerative capacity after injury is an important indicator of the muscle development process, reflecting

adaptability to external stimuli and self-repair abilities. To simulate muscle damage, we injected mice with CTX. In *flox* mice, qPCR analysis revealed a significant increase in *TNFα* expression induced by CTX, accompanied by the entire regeneration process (Figure 2N). MRI analysis further revealed a smaller injury area in *TNFα*-CKO mice 5 d after CTX-induced muscle injury (Figure 2O). Both H&E (Figure 2P) and IF staining (Figure 2Q) demonstrated that, compared to *flox* mice, *TNFα*-CKO mice exhibited more intact muscle fiber structures 3 or 5 d after CTX-induced injury. This was accompanied by a clearer laminin outline and the up-regulation of embryonic myosin heavy chain (eMyHC), a key marker of muscle regenerative capacity. These observations suggest that *TNFα*-CKO mice possess a stronger muscle regenerative ability than *flox* mice.

Functional validation of *TNFα* in primary myoblasts of *TNFα*-CKO mice

To confirm the *in vitro* function of *TNFα*, we established primary myoblasts from *flox* and *TNFα*-CKO mice. As expected, *TNFα* mRNA and protein levels were extremely low in the *TNFα*-CKO primary myoblasts (Figure 3A), which also exhibited a higher number of EdU$^+$ cells (Figure 3B) and significantly up-regulated *CDK4* and *Cyclin B* expression (Figure 3C). Bright-field microscopy also indicated that *TNFα* deletion facilitated the formation of myotubes following the induction of primary myoblast differentiation for 2 d (Figure 3D). Furthermore, IF staining further revealed that *TNFα*-CKO led to myotube hypertrophy, as demonstrated by the formation of a greater number of longer and thicker myotubes marked by *MyHC* (Figure 3E–H). Concurrently, the mRNA and protein levels of myogenic marker genes *MyHC*, *MyoG*, and *MyoD* were significantly up-regulated (Figure 3I, J). In summary, similar to our observations for C2C12 cells, deletion of *TNFα* significantly promoted the proliferation and differentiation of primary myoblasts.

Identification of new targets for *TNFα* in myoblast cells

Current understanding, such as *TNFα* facilitating NF-κB nuclear entry and activating certain MAP kinases, fails to fully elucidate the role of *TNFα* in myoblasts. To explore this further, we isolated the nucleus (N) and cytoplasm (C) of *flox* and *TNFα*-CKO primary myoblasts in the early stages of differentiation to identify new targets using label-free proteomic profiles. To illustrate changes in the distribution of differentially abundant proteins (DAPs; fold-change>1.5 or <0.67, *P*-value<0.05) between the cell nucleus and cytoplasm, we presented up-regulated and down-regulated proteins

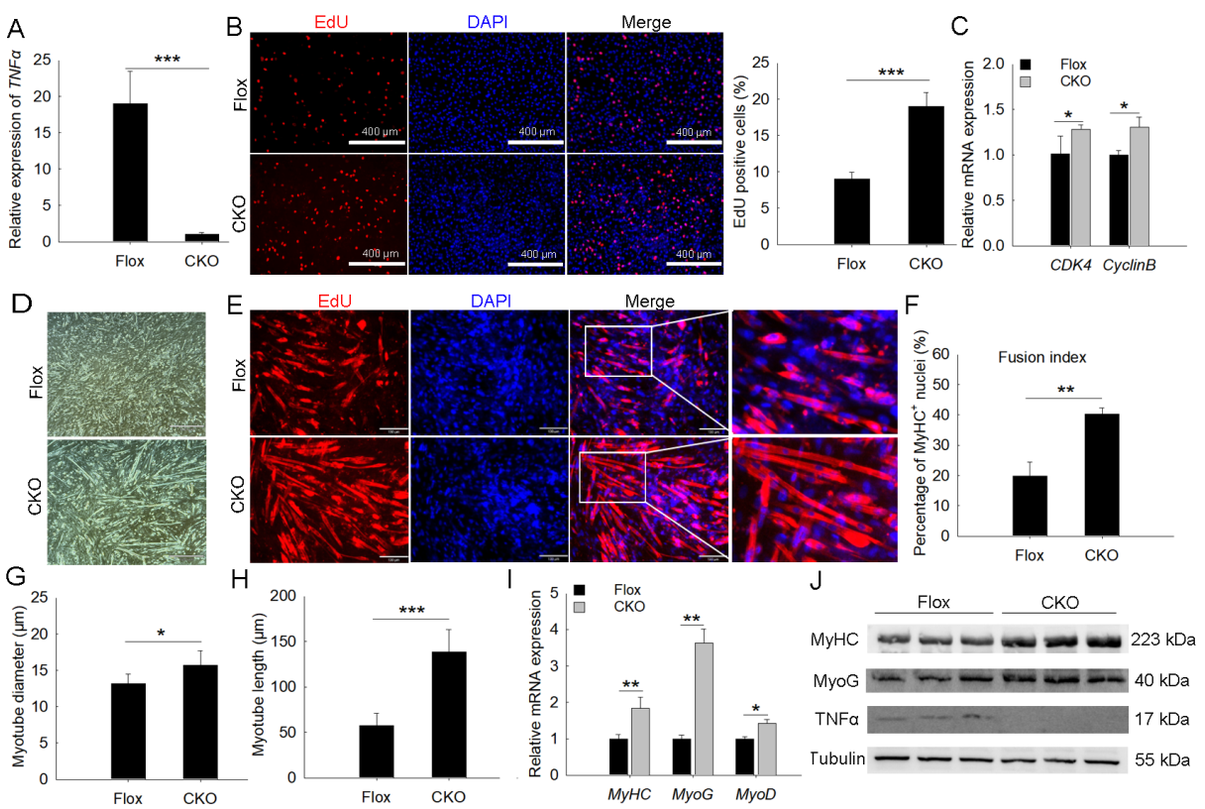

Figure 3 Functional verification of *TNFα* expression in primary myoblasts

A: Detection of *TNFα* mRNA level in *flox* and CKO primary myoblasts using qPCR. B: Representative photographs of EdU-stained *flox* and *TNFα*-CKO primary myoblasts. EdU$^+$ staining (red) of S-phase cells and DAPI staining (blue) of cell nuclei are shown (Scale bar: 400 μm), and proliferative cells were quantified as a ratio of EdU$^+$/DAPI$^+$. C: Analysis of expression levels of proliferation marker genes in *flox* and *TNFα*-CKO primary myoblasts using qPCR. Same number of *flox* and *TNFα*-CKO primary myoblasts were inoculated in plates and cultured in growth medium. D: Differentiation of primary myoblasts observed under a microscope 2 d after incubation in differentiation medium (Scale bar: 520 μm). E: Immunofluorescence staining of MyHC in *flox* and *TNFα*-CKO primary myoblasts 2 d after incubation in differentiation medium (Scale bar: 130 μm). Fusion index (F), myotube diameter (G), and myotube length (H) were quantified. I: Analysis of expression levels of myogenic marker genes in *flox* and *TNFα*-CKO primary myoblasts using qPCR. Myoblasts were differentiated for 2 d. J: Analysis of protein expression levels of MyHC, MyoG, and TNFα in *flox* and *TNFα*-CKO primary myoblasts. Myoblasts were differentiated for 2 d. Data are presented as mean±SD (n=3). *: P<0.05; **: P<0.01; ***: P<0.001 (Student's t-test).

separately. Most DAPs exhibited changes exclusively in either the cell nucleus or cytoplasm, while some exhibited synchronous changes in both compartments (Figure 4A). Notably, a small subset of DAPs, including six nucleus-down-regulated and cytoplasm-up-regulated proteins and one nucleus-up-regulated and cytoplasm-down-regulated protein, displayed a pattern reminiscent of translocation between the nucleus and cytoplasm (Figure 4A).

We used a heatmap to display changes in the abundances of selected proteins of interest, some of which may be potential targets of TNFα (Figure 4B). Compared to the *flox* group, Hira and Casz1 were significantly up-regulated in the nucleus of the *TNFα*-CKO group, with no detection in the cytoplasm, whereas Casp7, which was down-regulated, was only present in the cytoplasm. Arhgap10, up-regulated in the nucleus and down-regulated in the cytoplasm, exhibited the opposite shuttle direction to Gas1, which was down-regulated in the nucleus and up-regulated in the cytoplasm. Furthermore, Fgf21, Des, Igf2, and Igfbp5 were up-regulated in both the nucleus and cytoplasm, while fhl1, Pik3r1, and Myh4 were down-regulated in both compartments, implying corresponding changes in their total cellular levels. Map3k20, Cfl2, Tnni1, and Myom3 were significantly up-regulated, while Stat1, Stat2, Diaph1, Pdcd4, and Ripk1 were significantly down-regulated in the nucleus, with no significant changes in the cytoplasm (Figure 4B). These alterations in protein abundance in the cell nucleus suggest potential regulatory roles in myogenesis. Additionally, western blot analysis (Figure 4C) using Histone 3 and GAPDH as reference proteins for the nucleus and cytoplasm, respectively, confirmed the expression of several proteins related to muscle development. Densitometry on the western blot bands (Figure 4D) indicated that the changes in protein abundance closely matched the heatmap results, confirming the reliability of the proteomic data.

GSEA can assess the interactions between predefined gene lists and the standard hallmark collection, potentially uncovering biological pathways not limited to DAPs. As expected, *TNFα* deficiency resulted in negative enrichment of the TNF (normalized enrichment score (NES)=−1.89, *P*<0.001, FDR Q=0.004) and NF-κB (NES=−1.74, *P*=0.006, FDR Q=0.01) signaling pathways, accompanied by *TNFα*-induced apoptosis (NES=−2.12, *P*<0.001, FDR *Q*<0.001) (Supplementary Figure S2A). Furthermore, *TNFα* deficiency led to positive enrichment in MyoD targets (NES=2.39, *P*<0.001, FDR *Q*<0.001) (Figure 4E) and oxidative phosphorylation (NES=2.22, *P*<0.001, FDR *Q*<0.001) (Figure 4F). Conversely, it resulted in negative enrichment of the JAK-STAT signaling pathway (NES=−1.62, *P*=0.023, FDR Q=0.052) (Figure 4G). For instance, highly enriched and up-regulated DAPs, including Igf2, Igfbp5, Cfl2, Myh3, and Myl4, were identified in MyoD targets, while down-regulated DAPs,

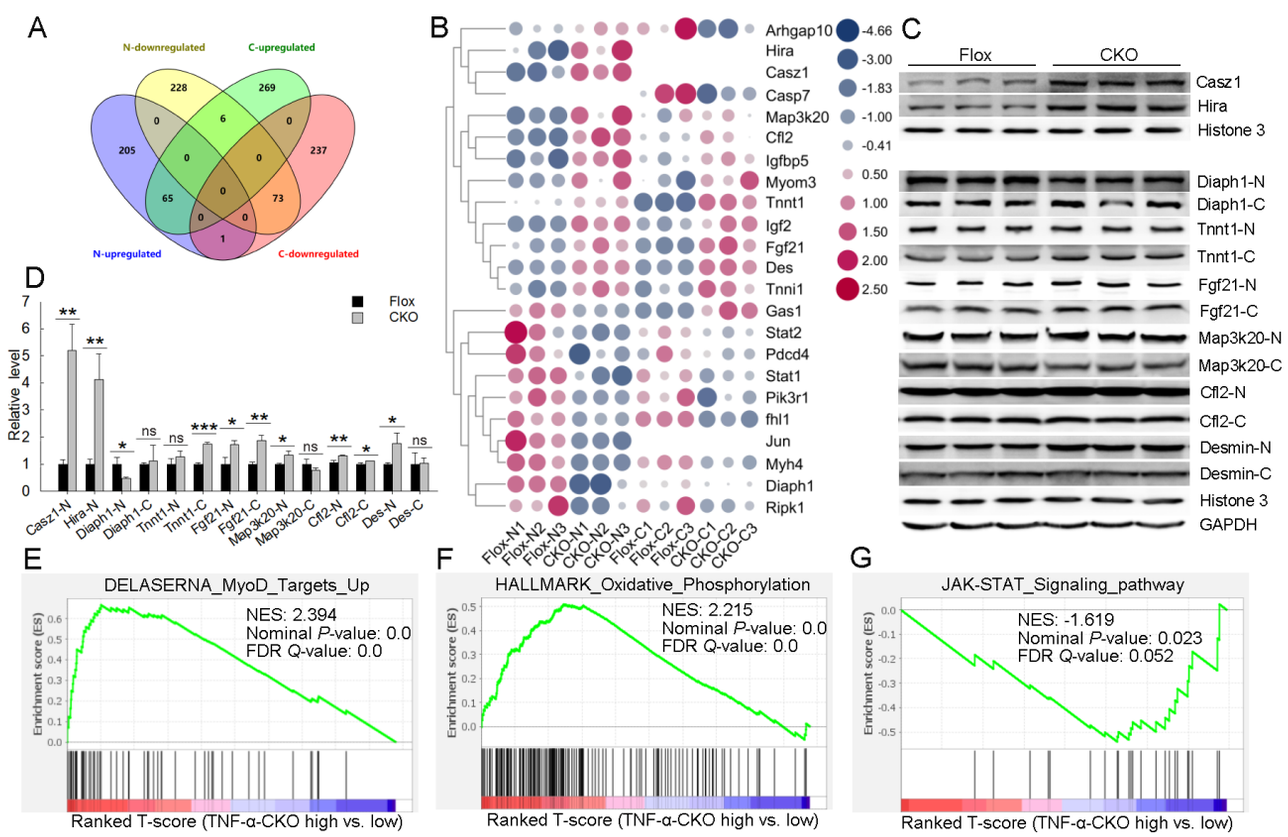

Figure 4 *TNFα*-CKO-induced changes in protein distribution and pathway enrichment

A: Venn diagram showing overlap between up-regulated and down-regulated differentially abundant proteins (DAPs) in nucleus (N) and cytoplasm (C) based on fold change>1.5 and *P*<0.05. B: Heatmap showing degree of changes in DAP levels due to *TNFα*-CKO. Scale size was normalized and shown by area. C: Western blots showing degree of changes in levels of certain proteins related to muscle development. *Flox* and *TNFα*-CKO primary myoblasts were induced to differentiate for 2 d. Histone 3 and GAPDH were used as reference proteins for N and C, respectively. Corresponding quantifications are shown in (D). Relative level indicates target protein/internal reference ratio of densitometry on western blot bands (*n*=3). Data are presented as mean±SD. *: *P*<0.05; **: *P*<0.01; ***: *P*<0.001 (Student's *t*-test). E–G: GSEA assays of proteomic data showing positive enrichment of MyoD targets and oxidative phosphorylation and negative enrichment of JAK-STAT signaling pathway following *TNFα*-CKO.

such as Jun, Stat1, Stat2, and Stat3, were observed in the JAK-STAT signaling pathway (Supplementary Figure S2B). These findings reveal novel *TNFα*-regulated targets and pathways that potentially mediate the effects of *TNFα* on muscle growth and development.

DISCUSSION

In this study, we explored the influence of *TNFα* on myoblast proliferation, migration, differentiation, and myotube fusion. Specifically, we assessed the effects of *TNFα*-CKO on muscle development and regeneration in mice, and identified novel *TNFα*-regulated targets and pathways, which may act as critical mediators in muscle development. These findings could significantly enhance our understanding of the role of *TNFα* in muscle development and provide a theoretical basis for molecular breeding and myopathy treatment.

Our results indicated that *TNFα* knockdown promoted the proliferation of C2C12 myoblasts, which was also confirmed in primary myoblasts. Previous studies have indicated that *TNFα* overexpression significantly reduces the number of $Pax7^+$ cells (Li et al., 2020), while exogenous TNFα protein can stimulate myoblasts and satellite cell proliferation (Alvarez et al., 2020; Li, 2003; Shirakawa et al., 2021). These contrasting results may be due to the differing effects of high and low TNFα concentrations on myoblast proliferation or suggest distinct mechanisms of action between exogenously administered and endogenous *TNFα*. Additionally, we demonstrated the role of *TNFα* in myoblast migration and established *TNFα*-CKO mice to investigate the effects of *TNFα* on muscle development and regeneration, which has not been previously reported. Results indicated that the *TNFα*-CKO mice exhibited enhanced muscle regeneration after CTX-induced injury, consistent with the phenotype observed in *TNFα* knock-in mice (Li et al., 2020) but in contrast to the muscle regeneration impairment observed in TNFα receptor double-knockout mice ($p55^{-/-}p75^{-/-}$) (Chen et al., 2005). These findings, combined with the results of cell proliferation analysis, suggest the involvement of both autocrine *TNFα* and receptor-mediated *TNFα* in muscle development. Furthermore, we observed that *TNFα*-CKO accelerated fat tissue deposition in skeletal muscles, without affecting the development of bones and visceral organs. We inferred that *TNFα*-CKO influenced lipid deposition through paracrine or endocrine mechanisms. Therefore, the *TNFα*-CKO mice established in this study may serve as valuable models for further research into the roles of *TNFα* in muscle development or other physiological effects.

Identifying new targets and pathways of *TNFα* in skeletal muscle is essential for understanding its regulatory mechanisms in muscle development. In this study, we found that *TNFα* deletion significantly up-regulated the levels of histone chaperone Hira and zinc finger transcription factor Casz1 in the cell nucleus. Previous studies have suggested that Hira knockout can significantly reduce histone variant H3.3 deposition and H3K27ac modification in muscle gene regulatory regions, thereby inhibiting myoblast proliferation, differentiation, and skeletal muscle development and regeneration (Valenzuela et al., 2017). Casz1 promotes skeletal muscle differentiation by directly affecting regional epigenetic modifications, chromatin accessibility, and super-enhancer establishment (Liu et al., 2020). GSEA has shown positive enrichment of MyoD targets following Casz1 overexpression (Liu et al., 2020), consistent with our results (Figure 4E). These findings suggest that the enhancement of muscle development following *TNFα* knockout partially depends on the biological functions of Hira and Casz1. Arhgap10, identified from genome-wide selection signals in meat from goat breeds, promotes myoblast proliferation and differentiation (Yuan et al., 2023). Our results showed that *TNFα* knockout induced Arhgap10 translocation from the cytoplasm to the nucleus, indicating its activation and nuclear function following *TNFα* knockout. Conversely, Gas1 exhibited the opposite translocation direction compared to Arhgap10. Gas1 has been shown to negatively impact skeletal muscle stem cells and muscle regeneration (Li et al., 2019), consistent with the stronger muscle regeneration capacity observed in *TNFα*-CKO mice in this study. Cfl2 is an essential mediator for myogenic differentiation in C2C12 cells (Nguyen et al., 2020), and its loss leads to abnormal sarcomere formation (Balakrishnan et al., 2020). Map3k20 and Diaph1 positively and negatively regulate myogenic differentiation, respectively, by affecting MyoG expression (Saleh et al., 2019; Yan et al., 2022). Our results showed that *TNFα* knockout also resulted in the up-regulation of Cfl2 and Map3k20 and the down-regulation of Diaph1, theoretically favoring myogenic differentiation. In addition, *TNFα*-CKO significantly up-regulated slow-twitch muscle fiber markers (mRNA level of *Myh7*, protein levels of Tnnt1 and Tnni1) and down-regulated the protein and mRNA levels of the fast-twitch muscle fiber marker *MYH4* (Figure 4B). These results align with the increased endurance observed in *TNFα*-CKO male mice. The absence of similar endurance improvements in female mice requires further investigation, as their phenotypic differences were also less pronounced compared to those in males.

Muscle fibers are highly metabolically active cells. During myogenic differentiation, myoblasts undergo autophagy-mediated mitochondrial remodeling, shifting from a highly glycolytic state to a pronounced reliance on oxidative phosphorylation (Sin et al., 2016). The significant positive enrichment in oxidative phosphorylation suggests that *TNFα* deficiency may affect the energy metabolism of myoblasts, in accordance with the relatively rigid structural demands imposed by muscle contraction. *TNFα* is known to significantly activate the JAK/STAT pathway in endothelial and microglial cells (Coelho-Santos et al., 2012; Kandhaya-Pillai et al., 2022). Typically, the JAK-STAT pathway inhibits myogenic differentiation (Jang & Baik, 2013). For instance, Stat1 interacts with MEF2, repressing its transcriptional activity and thereby suppressing myogenic differentiation (Xiao et al., 2011). Similarly, circ*SVIL*, *SOCS1*, *SOCS3*, and *PIAS1* promote myogenic differentiation by inhibiting the JAK-STAT pathway (Diao et al., 2009; Yue et al., 2022). Our results showed that *TNFα* deficiency led to negative enrichment in the JAK-STAT pathway, accompanied by decreased levels of Stat1, Stat2, and Stat3 in the cell nucleus, although the down-regulation of Stat1 was only 1.32-fold and did not meet differential criteria. Further research on the impact of *TNFα* on the phosphorylation of STAT proteins, or validation using activators and inhibitors of the JAK/STAT signaling pathway, may be beneficial. These findings provide initial insights into the relationship between *TNFα* and these pathways in skeletal muscle, offering new avenues for understanding the mechanisms by which *TNFα* regulates muscle development. These findings are integrated and presented in Figure 5.

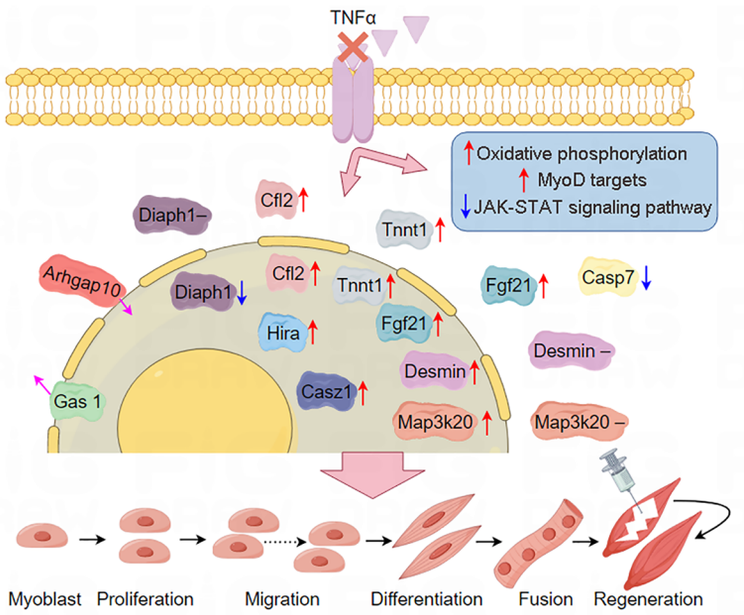

Figure 5 Diagram showing mechanism of action of *TNFα*-CKO in regulating muscle growth and development

Red and blue arrows indicate up-regulation and down-regulation of protein levels or pathway enrichment, respectively. Horizontal line indicates non-significant changes, pink arrow indicates direction of protein transfer. Figure was drawn by Figdraw.

SUPPLEMENTARY DATA

Supplementary data to this article can be found online.

COMPETING INTERESTS

The authors declare that they have no competing interests.

AUTHORS' CONTRIBUTIONS

Y.F. and H.Z. conceived and designed the study and supervised the analyses. Y.F. and X.H. prepared the data. X.H. analyzed the data. X.H. and J.R.N. prepared the draft of the manuscript. P.S., B.Z., and D.W.Y. provided resources. X.H., Y.F., and H.Z. revised and finalized the manuscript. All authors read and approved the final version of the manuscript.

ACKNOWLEDGMENTS

The authors are grateful to Dr. Kai Gao (Institute of Laboratory Animals Science, CAMS & PUMC) for assistance with MRI experiments.

REFERENCES

Alvarez AM, DeOcesano-Pereira C, Teixeira C, et al. 2020. IL-1β and TNF-α modulation of proliferated and committed myoblasts: IL-6 and COX-2-derived prostaglandins as key actors in the mechanisms involved. *Cells*, **9**(9): 2005.

Balakrishnan M, Yu SF, Chin SM, et al. 2020. Cofilin loss in *Drosophila* muscles contributes to muscle weakness through defective sarcomerogenesis during muscle growth. *Cell Reports*, **32**(3): 107893.

Bodine SC, Latres E, Baumhueter S, et al. 2001. Identification of ubiquitin ligases required for skeletal muscle atrophy. *Science*, **294**(5547): 1704–1708.

Chen SE, Gerken E, Zhang YM, et al. 2005. Role of TNF-α signaling in regeneration of cardiotoxin-injured muscle. *American Journal of Physiology-Cell Physiology*, **289**(5): C1179–C1187.

Chen SE, Jin BW, Li YP. 2007. TNF-α regulates myogenesis and muscle regeneration by activating p38 MAPK. *American Journal of Physiology-Cell Physiology*, **292**(5): C1660–C1671.

Coelho-Santos V, Gonçalves J, Fontes-Ribeiro C, et al. 2012. Prevention of methamphetamine-induced microglial cell death by TNF-α and IL-6 through activation of the JAK-STAT pathway. *Journal of Neuroinflammation*, **9**: 103.

Collins RA, Grounds MD. 2001. The role of tumor necrosis factor-alpha (TNF-α) in skeletal muscle regeneration: studies in TNF-α(-/-) and TNF-α(-/-)/LT-α(-/-) mice. *Journal of Histochemistry & Cytochemistry*, **49**(8): 989–1001.

Di Credico A, Gaggi G, Izzicupo P, et al. 2023. Betaine treatment prevents TNF-α-mediated muscle atrophy by restoring total protein synthesis rate and morphology in cultured myotubes. *Journal of Histochemistry & Cytochemistry*, **71**(4): 199–209.

Diao YR, Wang X, Wu ZG. 2009. SOCS1, SOCS3, and PIAS1 promote myogenic differentiation by inhibiting the leukemia inhibitory factor-induced JAK1/STAT1/STAT3 pathway. *Molecular and Cellular Biology*, **29**(18): 5084–5093.

Fang WY, Tseng YT, Lee TY, et al. 2021. Triptolide prevents LPS-induced skeletal muscle atrophy via inhibiting NF-κB/TNF-α and regulating protein synthesis/degradation pathway. *British Journal of Pharmacology*, **178**(15): 2998–3016.

Horiuchi T, Mitoma H, Harashima SI, et al. 2010. Transmembrane TNF-α: structure, function and interaction with anti-TNF agents. *Rheumatology (Oxford)*, **49**(7): 1215–1228.

Hsu H, Xiong J, Goeddel DV. 1995. The TNF receptor 1-associated protein TRADD signals cell death and NF-κB activation. *Cell*, **81**(4): 495–504.

Jang DI, Lee AH, Shin HY, et al. 2021. The role of tumor necrosis factor alpha (TNF-α) in autoimmune disease and current TNF-α inhibitors in therapeutics. *International Journal of Molecular Sciences*, **22**(5): 2719.

Jang YN, Baik EJ. 2013. JAK-STAT pathway and myogenic differentiation. *JAK-STAT*, **2**(2): e23282.

Kandhaya-Pillai R, Yang XM, Tchkonia T, et al. 2022. TNF-α/IFN-γ synergy amplifies senescence-associated inflammation and SARS-CoV-2 receptor expression via hyper-activated JAK/STAT1. *Aging Cell*, **21**(6): e13646.

Kriegler M, Perez C, DeFay K, et al. 1988. A novel form of TNF/cachectin is a cell surface cytotoxic transmembrane protein: ramifications for the complex physiology of TNF. *Cell*, **53**(1): 45–53.

Langen RCJ, Van Der Velden JLJ, Schols AMWJ, et al. 2004. Tumor necrosis factor-alpha inhibits myogenic differentiation through MyoD protein destabilization. *The FASEB Journal*, **18**(2): 227–237.

Li LJ, Rozo M, Yue SB, et al. 2019. Muscle stem cell renewal suppressed by GAS1 can be reversed by GDNF in mice. *Nature Metabolism*, **1**(10):

985–995.
Li JB, Yi XJ, Yao ZQ, et al. 2020. TNF receptor-associated factor 6 mediates TNFα-induced skeletal muscle atrophy in mice during aging. *Journal of Bone and Mineral Research*, **35**(8): 1535–1548.
Li YP. 2003. TNF-α is a mitogen in skeletal muscle. *American Journal of Physiology-Cell Physiology*, **285**(2): C370–C376.
Li YP, Schwartz RJ. 2001. TNF-α regulates early differentiation of C2C12 myoblasts in an autocrine fashion. *The FASEB Journal*, **15**(8): 1413–1415.
Liu ZH, Zhang XY, Lei HY, et al. 2020. CASZ1 induces skeletal muscle and rhabdomyosarcoma differentiation through a feed-forward loop with MYOD and MYOG. *Nature Communications*, **11**(1): 911.
Meyer SU, Thirion C, Polesskaya A, et al. 2015. TNF-α and IGF1 modify the microRNA signature in skeletal muscle cell differentiation. *Cell Communication and Signaling*, **13**: 4.
Nguyen MT, Min KH, Kim D, et al. 2020. CFL2 is an essential mediator for myogenic differentiation in C2C12 myoblasts. *Biochemical and Biophysical Research Communications*, **533**(4): 710–716.
Pasparakis M, Vandenabeele P. 2015. Necroptosis and its role in inflammation. *Nature*, **517**(7534): 311–320.
Sabio G, Davis RJ. 2014. TNF and MAP kinase signalling pathways. *Seminars in Immunology*, **26**(3): 237–245.
Saleh A, Subramaniam G, Raychaudhuri S, et al. 2019. Cytoplasmic sequestration of the RhoA effector mDiaphanous1 by Prohibitin2 promotes muscle differentiation. *Scientific Reports*, **9**(1): 8302.
Shirakawa T, Rojasawasthien T, Inoue A, et al. 2021. Tumor necrosis factor alpha regulates myogenesis to inhibit differentiation and promote proliferation in satellite cells. *Biochemical and Biophysical Research Communications*, **580**: 35–40.
Sin J, Andres AM, Taylor DJR, et al. 2016. Mitophagy is required for mitochondrial biogenesis and myogenic differentiation of C2C12 myoblasts. *Autophagy*, **12**(2): 369–380.
Subramanian A, Tamayo P, Mootha VK, et al. 2005. Gene set enrichment analysis: a knowledge-based approach for interpreting genome-wide expression profiles. *Proceedings of the National Academy of Sciences of the United States of America*, **102**(43): 15545–15550.
Valenzuela N, Soibam B, Li LR, et al. 2017. HIRA deficiency in muscle fibers causes hypertrophy and susceptibility to oxidative stress. *Journal of Cell Science*, **130**(15): 2551–2563.
Varfolomeev E, Vucic D. 2018. Intracellular regulation of TNF activity in health and disease. *Cytokine*, **101**: 26–32.
Xiao F, Wang HX, Fu XR, et al. 2011. Oncostatin M inhibits myoblast differentiation and regulates muscle regeneration. *Cell Research*, **21**(2): 350–364.
Yan JY, Yang YL, Fan XH, et al. 2022. circRNAome profiling reveals circFgfr2 regulates myogenesis and muscle regeneration via a feedback loop. *Journal of Cachexia, Sarcopenia and Muscle*, **13**(1): 696–712.
Yuan Y, Zhang WY, Yang BG, et al. 2023. A 1.1 Mb duplication CNV on chromosome 17 contributes to skeletal muscle development in Boer goats. *Zoological Research*, **44**(2): 303–314.
Yue BL, Yang HY, Wu JY, et al. 2022. circSVIL regulates bovine myoblast development by inhibiting STAT1 phosphorylation. *Science China Life Sciences*, **65**(2): 376–386.